STRUCTURAL INTEGRITY EVALUATION OF 3D PRINTED GRAPHENE-REINFORCED PLA NOTCHED PLATES USING FAILURE ASSESSMENT DIAGRAMS

Sergio Cicero[1], Sergio Arrieta[1], Marcos Sanchez[1]

[1] LADICIM, University of Cantabria, Santander, Cantabria, Spain

ABSTRACT

Failure Assessment Diagrams (FADs) constitute a well-known structural integrity evaluation tool that allows structural components containing crack-like defects to be assessed through a simultaneous analysis of fracture and plastic-collapse processes. FADs are included in the most recognized structural integrity assessment procedures/standards, such as BS7910 and API 579/ASME FFS-1, and their use is generally limited to metallic components containing crack-like defects.

On the other hand, structural responsibilities are being assumed by 3D printed composites, and particularly by those obtained through FFF (Fused Filament Fabrication), beyond their most extended use as prototyping materials. The resulting structural components may contain notch-type defects (e.g., grooves, corners, holes, etc.) that determine their corresponding structural integrity. Thus, it is necessary to define structural integrity assessment criteria for this kind of materials when containing any kind of stress risers, beyond crack-like defects.

This work justifies the use of BS7910 Level 1 FAD, coupled with a notch correction derived from the Theory of Critical Distances (TCD), to analyze graphene-reinforced PLA plates subjected to pure tensile loading conditions and containing U- and V-notches. The results reveal that, for U- and V-notches, the assessment points representing the plates at failure are located within the FAD area corresponding to unsafe conditions, providing conservative evaluations with moderate safety margins. For plates containing circular holes, the proposed approach provides unsafe predictions.

Keywords: structural integrity, composite, defect, fracture, toughness, failure.

NOMENCLATURE

B	Specimen thickness
E	Young´s modulus
K_{mat}	material fracture toughness in stress intensity factor units
K^N_{mat}	material fracture resistance in notched conditions (in stress intensity factor units)
K_r	fracture ratio of applied KI to fracture toughness
K_I	applied stress intensity factor
L_r	ratio of applied load to limit load (or reference stress to yield stress)
$L_{r,max}$	maximum value of Lr in a FAD
P	applied load
P_{est}	estimation of the load bearing capacity (estimated critical load)
P_{exp}	experimental load bearing capacity (experimental critical load)
P_L	limit load
J	applied J-integral
J_e	elastic component of J
L	critical distance
ρ	notch radius
σ_{ref}	reference stress
σ_u	ultimate tensile strength
σ_y	yield stress
σ_Y	flow stress (average of σ_y and σ_u)
σ_0	inherent strength
AM	Additive Manufacturing
FAD	Failure Assessment Diagram
FAL	Failure Assessment Line
FFF	Fused Filament Fabrication
PLA	Polylactic acid
PLA-Gr	Graphene reinforced PLA
LM	Line Method

TCD Theory of Critical Distances

1. INTRODUCTION

The assessment of structural components containing crack-like defects is usually made by applying structural integrity assessment procedures (e.g., BS7910 [1], API 579-1/ASME FFS-1 [2]) that are generally based on Failure Assessment Diagrams (FADs). Such diagrams allow a simultaneous analysis of fracture and plastic collapse processes which is performed through two normalized parameters, K_r and L_r:

$$K_r = \frac{K_I}{K_{mat}} \tag{1}$$

$$L_r = \frac{P}{P_L} = \frac{\sigma_y}{\sigma_{ref}} \tag{2}$$

where K_I is the stress intensity factor, K_{mat} is the material fracture toughness in stress intensity factor units, P is the applied load, P_L is the limit load, σ_y is the material yield stress and σ_{ref} is the reference stress. Assessment procedures provide analytical solutions for K_I and P_L (or σ_{ref}) for a wide variety of component and crack geometries. Looking at equations (1) and (2), it can be easily inferred that K_r evaluates the component against fracture and L_r evaluates the component against plastic collapse, with both defining the resulting assessment point within the FAD. The location of the point is finally compared with the critical conditions defined by the Failure Assessment Line (FAL): when the assessment point is located above the FAL, the component is assumed to be under unsafe conditions, whereas if the assessment point is located between the FAL and the coordinate axes, the component is assumed to be under safe conditions. Finally, failure conditions are achieved when the assessment point lies just on the FAL [1,2]. Figure 1 shows and example of FAD assessment where the assessment point indicates that the component is in unsafe conditions.

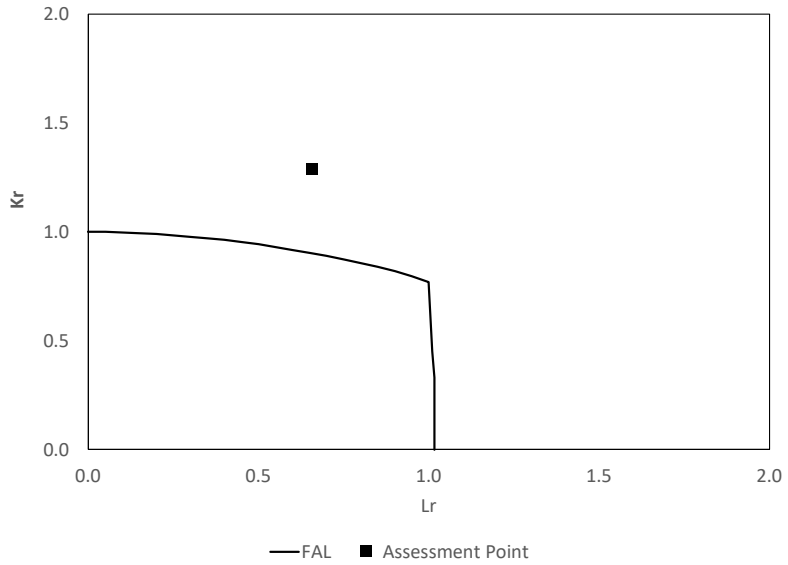

FIGURE 1: EXAMPLE OF FAD ASSESSMENT, SHOWING THE FAILURE ASSESSMENT LINE AND THE ASSESSMENT POINT.

In practice, nevertheless, there are frequent situations (e.g., mechanical damage, corrosion defects, holes, weld toes, structural connections, etc.) where the defects or the structural details jeopardizing the integrity of a particular structural component are not crack-like defects. In such cases, it may be too conservative to assume that they behave like cracks and, then, to apply fracture mechanics criteria. The literature demonstrates (e.g., [3-6]) how components with non-sharp defects (here referred to as notches) develop an apparent fracture toughness (K^N_{mat}) which is greater than that developed in cracked conditions, something that has direct implications on the resulting load-bearing capacity. Thus, the analysis of the fracture behavior of notched materials can be performed using different criteria (e.g., [3,7]), among which the Theory of Critical Distances (TCD) has been widely described and validated. Moreover, the TCD may be used to generate structural integrity assessment criteria for components containing notch-type defects, as proposed in [8] by combining FADs with this particular theory.

Furthermore, structural integrity assessment procedures (e.g., [1,2]) generally address the evaluation of metallic materials, not covering non-metallic materials. However, Fused Filament Fabrication (FFF), framed within additive manufacturing (AM), is a

technology that allows complex geometries to be fabricated and it is applicable to a wide variety of materials, covering not only metals, but also polymers, ceramics and composites. When using FFF, a melted filament is extruded through a heated nozzle, which is then deposited on a build platform layer by layer until the final component is fabricated [9]. To date, FFF of polymers and polymer-matrix composites has been essentially used for prototyping, but not for components with structural duties, mainly because the obtained mechanical properties are commonly lower than those achieved when using more traditional fabrication methods (e.g., injection or extrusion). With the aim of improving the mechanical performance of FFF parts, there have been significant research efforts to improve the knowledge about this technique and the resulting printed materials (e.g., [9-14]), which have been used already to build final components such as vessels, pipes or flanges (e.g., [15,16]). Consequently, FFF polymer matrix (composite) materials are increasingly assuming structural responsibilities and there is a need for specific structural integrity assessment procedures for this kind of materials when containing crack-like defects and notches. In this sense, some research has provided FAD assessments of non-metallic materials containing cracks (e.g., [17,18]) but, to the best knowledge of the authors, there is just one work [19] analyzing the use of FADs and the TCD in the assessment of FFF notched polymers and polymer-matrix composites, with such research being strictly focused on typical (SENB) fracture mechanics specimens, subjected to a different type of loading and constraint conditions, and another work [20] applying the same approach to FFF notched structural plates made of polymer PLA.

With all this, this work analyzes the structural integrity of FFF graphene-reinforced PLA plates containing different types of U- and V-shaped notches, addressing two main issues: the analysis of notch-type defects in plates subjected to tensile loads, using FADs together with the TCD, and; the application of FADs to a particular (non-metallic) FFF polymer-matrix composite. The obtained results demonstrate that the proposed approach generates safe, reasonably conservative structural integrity assessments on this particular combination of component geometry, loading conditions and material.

2. MATERIALS AND METHODS

2.1 Materials

The material investigated in this work is FFF graphene-reinforced (1 wt.%) PLA, PLA-Gr, supplied as filaments to be directly used in the FFF printing process. The material tensile and fracture properties are analyzed in a previous work (see [21] for details), and the main mechanical properties are collected in Table 1.

TABLE 1: TENSILE AND FRACTURE PROPERTIES. E: YOUNG'S MODULUS; σ_Y: YIELD STRESS; σ_u: ULTIMATE TENSILE STRENGTH; ε_u: STRAIN UNDER MAXIMUM LOAD. TCD PARAMETERS. L: CRITICAL DISTANCE; σ_0: INHERENT STRENGTH.

E (MPa)	σ_y (MPa)	σ_u (MPa)	ε_u (%)	L (mm)	K_{mat} (MPam$^{1/2}$)
3972	47.5	49.0	1.5	1.06	7.2

The printed plates were all manufactured by FFF using a Prusa i3 printer, following the same process defined for the tensile and fracture specimens used in the basic characterization of the material [21], thus with the following printing parameters: nozzle diameter 0.4 mm; nozzle temperature 200 ºC; bed temperature 75 ºC; printing rate 30 mm/s; infill level 100%; layer height 0.3 mm. In all cases, the specimens were printed with raster orientation 45/-45. The resulting plates have an anisotropic behavior, but as long as the plates are (tensile) loaded in the same direction as the tensile and fracture specimens (i.e., 0º direction), there is just one direction of interest in this research and anisotropy is not considered. Moreover, as seen in [21], the printed material presents internal microscopic voids with sizes around 50 μm, in spite of the infill level (100%) used during the printing process. Here, it is important to note that the effect of such defects on the mechanical behaviour of the printed composite is considered through the mechanical properties gathered in Table 1, which were obtained on specimens with the same microscopic voids. This allows the structural integrity analysis to be strictly focused on the macroscopic notches, whose size (as shown below) is several orders of magnitude larger than the internal voids.

The notches were all machined by milling after the printing process, as machined defects tend to provide higher strengths than printed defects [22] and, additionally, they do not include additional anisotropy around the notch tip.

The total number of tested plates was 51, combining three types of macroscopic notches (U-notches, V-notches, and circular holes), 2 different nominal notch radii (ρ = 0.9 mm and 1.3 mm), two nominal specimen widths (W = 60 mm and 120 mm), three specimen thicknesses (B = 5 mm, 10 mm, and 20 mm), and two notch lengths to specimen width ratios (a/W= 0.25 and 0.50). A schematic of the specimens is shown in Figure 2, with the actual geometrical values (slightly different to the nominal ones, and measured in the middle section), being shown in Table 2.

The loading rate was 1 mm/min for all the notched plates, which is the same rate used in [21] for the basic tensile and fracture characterization. The load vs. displacement curve was recorded for each test, determining the corresponding critical load (P_{exp}) (see Table 2). Figure 3 shows an example of the experimental setup.

2.2 Methods

This work provides the FAD assessment of FFF PLA-Gr plates containing notches. In this sense, there are two main issues: first, the use of the FAD methodology on notches, instead of crack-like defects, and; secondly, the use of the FAD methodology to analyze a non-metallic material.

Going back to ordinary FAD assessments, as outlined in the introduction, the limiting condition is established by the FAL. This line follows expressions which are functions of L_r:

$$K_r = f(L_r) \tag{3}$$

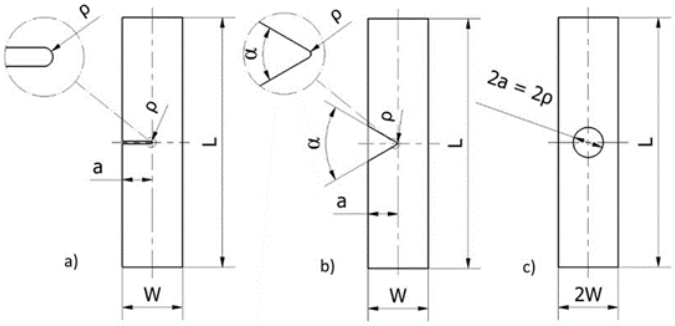

FIGURE 2: SCHEMATIC OF THE TESTED SPECIMENS. a) U-NOTCHED SPECIMENS; b) V-NOTCHED SPECIMENS; c) SPECIMENS WITH CENTRAL HOLE.

FIGURE 3: EXPERIMENTAL SETUP FOR SPECIMEN G210 (U-NOTCHED SPECIMEN, NOTCH RADIUS 0.89 mm, THICKNESS 10.14 mm, a/W = 0.25)

The different f(L_r) functions are actually plasticity corrections to the linear-elastic fracture assessment, whose exact solution is:

$$f(L_r) = \sqrt{\frac{J_e}{J}} \tag{4}$$

J being the applied J-integral and J_e being the elastic component of J. The use of $f(L_r)$ solutions as the FAL allows the linear-elastic stress intensity factor (K_I) to be used even in elastic-plastic situations and, thus, in combination with K_{mat} values associated with materials developing elastic-plastic fracture behavior. In other words, when performing a FAD analysis, although the linear-elastic K_I is used to account for the effect of the external loading and crack geometry, the final assessment may be elastic-plastic when using the $f(L_r)$ solutions as the limiting conditions.

In reality, structural integrity assessment procedures (e.g., [1,2]) offer approximate solutions to (4), which are defined through the tensile properties of the material and are normally provided hierarchically, with distinct levels of approximation to equation (4) depending on the level of detail in the definition of the tensile curve. With all this, the FAD methodology requires defining K_r, L_r and $f(L_r)$ (equations (1) to (4)).

TABLE 2: EXPERIMENTAL PROGRAM: GEOMETRICAL PARAMETERS, EXPERIMENTAL CRITICAL LOADS (P_{exp}), K_r AND L_r COORDINATES, AND RESULTING CRITICAL LOAD ESTIMATIONS (P_{est}) DERIVED FROM FAD ANALYSIS.

Notch	Specimen	a (mm)	W (mm)	ρ (mm)	B (mm)	P_{exp}(kN)	K_r	L_r	P_{est} (kN)	P_{est}/P_{exp}
U-notch	G201	30.60	60.51	0.86	4.85	3.87	1.49	1.29	2.30	0.59
	G202	30.84	60.38	0.91	4.88	3.86	1.51	1.31	2.25	0.58
	G203	30.73	60.50	0.83	4.85	3.89	1.52	1.31	2.25	0.58
	G204	30.66	60.46	0.87	10.02	8.52	1.60	1.37	4.60	0.54
	G205	30.59	60.46	0.88	9.96	8.54	1.60	1.38	4.60	0.54
	G206	30.83	60.49	0.86	9.98	8.76	1.67	1.43	4.60	0.52
	G207	31.02	120.36	0.81	4.96	10.55	1.07	0.66	9.00	0.85
	G208	30.34	120.31	0.83	4.98	13.15	1.29	0.80	9.20	0.70
	G209	30.58	120.20	0.89	4.97	10.14	1.00	0.63	9.20	0.91
	G210	31.02	120.36	0.89	10.14	24.43	1.20	0.74	19.00	0.78
	G211	30.92	120.43	0.84	10.13	26.41	1.30	0.80	19.00	0.72
	G212	31.06	120.48	0.88	10.00	23.07	1.15	0.71	18.50	0.80
	G213	31.08	120.43	0.88	20.17	39.90	0.98	0.57	37.00	0.93
	G214	31.25	120.62	0.89	20.05	42.56	1.06	0.62	37.00	0.87
	G215	30.83	120.63	0.87	20.14	47.30	1.16	0.68	37.00	0.78
	G301	30.85	60.48	1.24	4.86	3.69	1.39	1.23	2.30	0.62
	G302	30.98	60.40	1.24	4.91	4.29	1.63	1.44	2.30	0.54
	G303	30.91	60.54	1.26	4.77	3.80	1.47	1.30	2.30	0.60
	G304	30.85	60.47	1.26	9.96	8.63	1.59	1.38	4.65	0.54
	G305	31.19	60.55	1.27	9.92	8.60	1.62	1.41	4.60	0.53
	G306	30.95	60.47	1.25	9.93	8.40	1.56	1.36	4.60	0.55
	G307	30.62	120.32	1.26	4.88	11.51	1.12	0.71	9.60	0.83
	G308	30.93	120.30	1.27	4.92	11.21	1.09	0.69	9.60	0.86
	G309	30.92	120.42	1.26	4.94	11.46	1.11	0.70	9.60	0.84
	G310	31.02	120.25	1.27	9.96	25.37	1.22	0.77	19.00	0.75
	G311	31.04	120.33	1.26	9.93	22.38	1.08	0.69	19.00	0.85
	G312	31.08	120.43	1.26	9.93	26.31	1.27	0.80	19.00	0.72
V-notch	G401	27.03	60.56	1.25	4.76	4.27	1.27	1.10	2.95	0.69
	G402	26.87	60.54	1.05	4.80	4.09	1.21	1.03	2.95	0.72
	G403	26.99	60.49	0.89	4.83	4.58	1.38	1.16	2.95	0.64
	G404	26.95	60.60	0.65	9.92	9.56	1.43	1.15	6.00	0.63
	G405	26.92	60.55	0.93	9.99	10.04	1.45	1.20	6.00	0.60
	G406	26.93	60.58	0.87	9.92	8.76	1.28	1.06	6.00	0.68
	G407	26.95	120.24	1.07	4.89	10.65	0.93	0.61	10.50	0.99
	G408	26.50	120.26	1.15	4.83	10.30	0.89	0.59	10.50	1.02
	G409	26.80	120.33	1.01	4.86	12.05	1.06	0.69	10.50	0.87
	G410	26.96	120.46	0.97	9.94	24.25	1.05	0.68	21.00	0.87
	G411	26.92	120.29	0.89	9.95	25.32	1.11	0.71	21.00	0.83
	G412	26.87	120.53	1.05	9.95	24.10	1.03	0.68	21.00	0.87
Hole	G101	30.39	60.56	15.03	4.85	5.45	0.31	0.79	7.00	1.28
	G102	30.15	60.36	14.99	4.94	5.18	0.29	0.73	7.20	1.39
	G103	30.23	60.45	15.04	4.83	5.55	0.32	0.80	7.00	1.26
	G104	30.18	60.46	14.83	10.04	11.95	0.33	0.83	14.50	1.21
	G105	30.12	60.58	14.83	9.99	11.38	0.32	0.79	14.50	1.27
	G106	30.17	60.53	14.87	10.02	11.45	0.32	0.79	14.50	1.27
	G107	30.22	120.28	14.99	4.86	15.07	0.38	0.73	21.00	1.39
	G108	30.20	120.35	14.92	4.94	14.62	0.36	0.69	21.50	1.47
	G109	30.26	120.37	15.04	4.93	14.01	0.35	0.66	21.50	1.53
	G110	30.14	120.34	14.93	9.98	32.28	0.40	0.75	42.90	1.33
	G111	30.01	120.23	14.99	9.90	32.23	0.40	0.76	42.90	1.33
	G112	29.90	120.26	15.01	9.90	32.04	0.40	0.75	42.90	1.34

Now, regarding the FAD assessments to be used in this research, it is possible to use the FAD methodology, proposed in structural integrity assessment procedures for the analysis of crack-like defects, to the notch-type defects analyzed here. This requires that the real situation, with a notch type defect, is treated as an equivalent situation with a crack-like defect. This proposal [8] is based on the following assumption:

- a given notched component may be analyzed as if it was cracked, with the crack having the same dimensions as the notch (except for the radius at the defect tip), but with a larger material fracture resistance (the apparent fracture toughness, K^N_{mat}) than that developed in cracked conditions (the fracture toughness, K_{mat}). In other words, K_r has to be modified to account for the possible increase in the fracture resistance, using K^N_{mat} instead of K_{mat}. K_I solutions provided for cracked solutions remain valid for the notched situation, as it is being analyzed through an equivalent cracked situation.
- The notch effect is very limited in the limit load (P_L) and in the reference stress (σ_{ref}), as shown in [23]. Therefore, when analyzing notched components, the definition of the L_r coordinate is the same as that used in cracked conditions.
- The exact solution of the FAL may be applied in notched conditions. This was demonstrated in [24], where a very weak dependence of equation (4) (exact solution) on the notch radius was revealed.

These three considerations solve the first problem mentioned above: notches may be analyzed through FADs using equation (4) and by simply considering an appropriate value of K^N_{mat}.

- Finally, concerning the use of FADs to analyze non-metallic materials, in [17] it was firstly shown how the approximations to equation (4) provided by structural integrity assessment procedures, based on the material tensile properties, were rather conservative (i.e., safe) for a wide range of non-metallic structural materials, covering polymers, composites, and rocks. This solves the second issue and supports the possibility of analyzing the PLA-Gr notched plates analyzed here by using the FAD approaches defined in structural integrity assessment procedures, both those based on the exact solution of the FAL and those based on approximations based on the tensile behavior.

The only pending requirement is the definition of the apparent fracture toughness (K^N_{mat}) which, in this work, will be estimated through the TCD and, particularly, through the Line Method (LM).

Concerning the TCD, it includes different methodologies [3] which, when dealing with fracture assessments, make use of a material length parameter (the critical distance, L) together with the material fracture toughness. L is defined by:

$$L = \frac{1}{\pi}\left(\frac{K_{mat}}{\sigma_0}\right)^2 \tag{5}$$

where σ_0 is the material inherent strength. Of the different TCD methods, this work makes use of the line method (LM), which assumes that fracture takes place when the average stress along a distance equal to 2L (measured from the notch tip), reaches σ_0:

$$\frac{1}{2L}\int_0^{2L}\sigma(r)dr = \sigma_0 \tag{6}$$

The LM can generate predictions of the apparent fracture toughness (K^N_{mat}) developed by components containing U-shaped notches [3]. Combining equation (6) with the stress distribution, $\sigma(r)$, on the notch tip provided by Creager and Paris (equation (7)) [25], the apparent fracture toughness (K^N_{mat}) is given by equation (8):

$$\sigma(r) = \frac{K_I}{\sqrt{\pi}}\frac{2(r+\rho)}{(2r+\rho)^{3/2}} \tag{7}$$

$$K^N_{mat} = K_{mat}\sqrt{1+\frac{\rho}{4L}} \tag{8}$$

Creager-Paris stress distribution is equal to that ahead of the crack tip but displaced a distance equal to $\rho/2$ along the mid-plane axis, with K_I in equation (7) being the mode I stress intensity factor, ρ being the notch radius and r being the distance existing from the notch tip to the point being assessed.

The solution provided by equation (8) is based on the Creager-Paris equation. Thus, it is valid within the validity range of the Creager-Paris stress distribution, which is limited to slender U-notches. Their use on the V-notches with opening angle (α) of 60° is justified by the fact that such an opening angle provides a similar behavior to U-notches with α=0° (according to [26], critical loads are very similar as long as α is below 90º). Finally, in the case of central holes, with less demanding stress fields, equation (8) is clearly outside its validity range.

Consequently, the only notch correction required to use the FAD methodology in the analyses performed in this work is made on the K_r parameter, which is finally defined as:

$$K_r = \frac{K_I}{K_{mat}^N} = \frac{K_I}{K_{mat}\sqrt{1+\frac{\rho}{4L}}} \tag{9}$$

Summarizing, the assessment process is as follows (steps a) to d):

a) Calculate K_r following equation (9). Given that the notches in the real material are considered to behave as cracks in a tougher material, K_I values are determined for the corresponding critical load ($P = P_{exp}$, see Table 2) using the analytical solutions provided by [27] for edge cracks in finite plates (equation (10)) in the case of U-notch and V-notch analyses, and for through thickness cracks in finite plates (equation (11)) in the case of holes. Additionally, the notch effect is considered through K^N_{mat}, which is calculated following equation (9) for the notch radius (ρ) being analyzed, and using the K_{mat} and L values shown in Table 1 [21].

$$K_I = \frac{P}{B\sqrt{W}}\left[\left\{\frac{\sqrt{2\cdot tan\left(\frac{\pi a}{2W}\right)}}{cos\left(\frac{\pi a}{2W}\right)}\right\}\cdot\left\{0.752 + 2.02\left(\frac{a}{W}\right) + 0.37\left(1 - sin\left(\frac{\pi a}{2W}\right)\right)^3\right\}\right] \tag{10}$$

$$K_I = \frac{P}{B\sqrt{W}}\left[\sqrt{\frac{\pi a}{4W}sec\left(\frac{\pi a}{2W}\right)}\cdot\left\{1 - 0.025\left(\frac{a}{W}\right)^2 + 0.06\left(\frac{a}{W}\right)^4\right\}\right] \tag{11}$$

b) Calculate L_r following equation (2), with no need for any notch correction. Thus, P_L solutions provided by [27] for edge cracks (in the case of U- and V-notches, equation (12)) and through thickness cracks (in the case of holes, equation (13)) in finite plates will be used here. The value of P used to define L_r is the corresponding P_{exp} (again, see Table 2).

$$P_L = 1.455\cdot\left(\sqrt{1+\left(\frac{a}{b}\right)^2} - \frac{a}{b}\right)B\cdot b\cdot\sigma_Y \qquad (plane\ strain) \tag{12a}$$

$$P_L = 1.072\cdot\left(\sqrt{1+\left(\frac{a}{b}\right)^2} - \frac{a}{b}\right)B\cdot b\cdot\sigma_Y \qquad (plane\ stress) \tag{12b}$$

$$P_L = \frac{4}{\sqrt{3}}\cdot B\cdot b\cdot\sigma_Y \qquad (plane\ strain) \tag{13a}$$

$$P_L = 2\cdot B\cdot b\cdot\sigma_Y \qquad (plane\ stress) \tag{13b}$$

In all cases, b is the remaining ligament (W-a), and σ_Y is the flow stress, normally taken as the average between the yield stress, σ_y, and the ultimate tensile strength, σ_u, to take into account material hardening. However, when using FAD analysis where the proper Failure Assessment Line (FAL) includes de effect of material hardening in the definition of the cut-off ($L_{r,max}$, see below), σ_Y must be equal to σ_y, avoiding double counting the hardening of the material.

Here, it should be noted that there may be notched plates (those with nominal B = 20 mm) in a transitional situation between plane stress and plane strain conditions. In such cases, the P_L values were obtained from the linear interpolation between the plane stress and plane strain solutions of P_L provided by [27], with the interpolation limits being established by equations (14) and (15) for plane strain and plane stress conditions, respectively [3].

$$B \geq 2.5\left(\frac{K_{mat}^N}{\sigma_y}\right)^2 \tag{14}$$

$$B \leq \frac{1}{\pi}\left(\frac{K_{mat}^N}{\sigma_y}\right)^2 \tag{15}$$

c) Define the FAL. In this case, BS7910 Option 1 will be used. This FAL is an approximation to equation (4) providing an excellent balance between accuracy and simplicity. Equations (16) to (21) define this FAL. It can be observed how the whole FAL (K_r-L_r curve) may be defined from the material tensile properties (E, σ_y, σ_u), provided in Table 1:

$$K_r = f(L_r) = \left[1 + \frac{1}{2}(L_r)^2\right]^{-1/2} \cdot \left[0.3 + 0.7 \cdot e^{-\mu \cdot (L_r)^6}\right] \quad \text{if } L_r \leq 1 \tag{16}$$

$$K_r = f(L_r) = f(1) \cdot L_r^{\frac{N-1}{2N}} \quad \text{for } 1 < L_r \leq L_{r,max} \tag{17}$$

$$K_r = f(L_r) = 0 \quad \text{for } L_r = L_{r,max} \tag{18}$$

$$\mu = min\left[0.001 \cdot \frac{E}{\sigma_y}; 0.6\right] \tag{19}$$

$$N = 0.3 \cdot \left(1 - \frac{\sigma_y}{\sigma_u}\right) \tag{20}$$

$$L_{r,max} = \frac{\sigma_y + \sigma_u}{2 \cdot \sigma_y} \tag{21}$$

Equations (19) and (20), defining μ and N, have been validated by the authors in [17] for polymers, composites and rocks, and in [19] for additively manufactured polymers and composites.

d) Evaluate the situation (i.e., safe vs. unsafe) of the assessment point, with coordinates (K_r, L_r), regarding the FAL.

3. RESULTS AND DISCUSSION

Figure 4 shows examples of load-displacement curves obtained in different plates, revealing how plates with circular holes develop higher critical loads than U-notched and V-notched plates. Additionally, for a given type of defect (e.g., U-notch) there is a negligible effect of the notch radius (less than 2%, when taking average values) on the critical load and, finally, the differences between the critical loads in U-notched plates and V-notched plates (with the rest of geometrical parameters being equal or similar) are very minor. This last observation justifies the use of equation (8) also in V-notched plates with α=60º. Figure 5 shows an example of the broken plates after the tensile test.

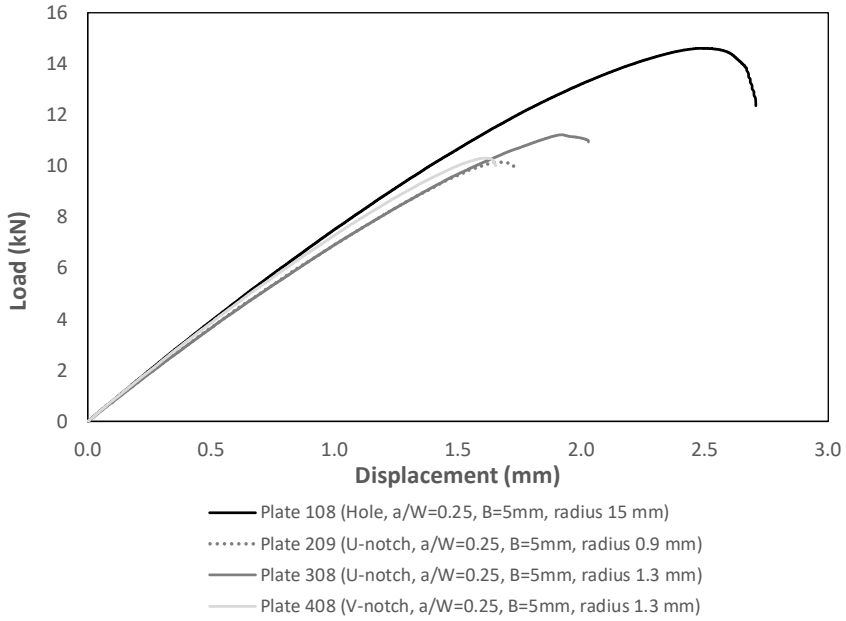

FIGURE 4: EXAMPLES OF LOAD-DISPLACEMENT CURVES OBTAINED IN PLATES CONTAINING DIFFERENT TYPES OF DEFECTS. GEOMETRICAL PARAMETERS REFER TO NOMINAL VALUES.

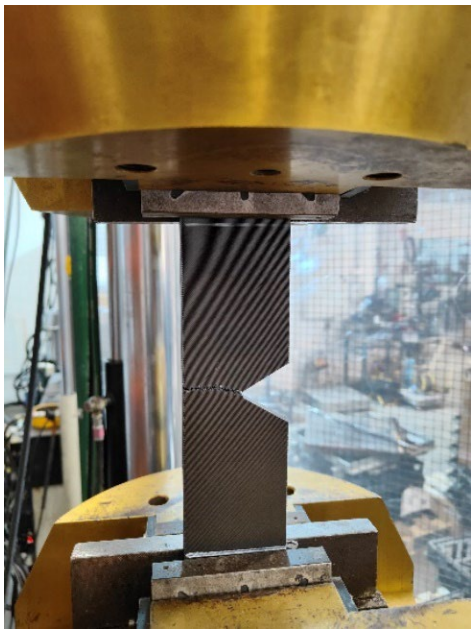

FIGURE 5: EXAMPLE OF TESTED PLATE AFTER FAILURE (PLATE G405).

With the corresponding critical load (i.e., maximum load in the load-displacement curve) of each plate, K_r and L_r were calculated as explained in Section 2. Table 2 gathers the resulting (K_r, L_r) coordinates of the different tested plates, with figures 6 to 8 showing the resulting FADs. The figures also shown the lines corresponding to $K_r/L_r = 0.4$, below which, failures are plastic collapse dominated, and to $K_r/L_r=1.1$, above which fracture dominates the failure process [28].

Table 2 also gathers the predicted critical loads (P_{est}), which are calculated as follows (see Figure 6a): the critical load, for each plate, corresponds to that one generating an assessment point that it is situated exactly on the FAL (point B). Therefore, and provided that the defect length (a) is constant during the loading process, the corresponding iso-a lines (for increasing levels of applied load) are straight lines with P_{est} being directly obtained from equation (22) (C being the assessment point for P_{exp}):

$$P_{est} = P_{exp} \cdot \frac{\overline{OB}}{\overline{OC}} \tag{22}$$

Finally, Table 2 also shows the resulting P_{est}/P_{exp} ratios.

In figures 6 (U-notches) and 7 (V-notches) it can be observed that 97.4% of the assessment points (38 of 39) are located above the FAL, meaning that the assessment points at failure are correctly located in the unsafe area. The further away the points are from the line, the more conservative the analysis is. This can be easily quantified through the P_{est}/P_{exp} ratios: the assessments points at failure located far from the FAL lead to low P_{est}/P_{exp} ratios, whereas such ratios increase as the assessment point approaches the FAL. Moreover, P_{est}/P_{exp} becomes 1 in those situations where the predicted load coincides with the experimental load, and is higher than 1 when the assessment point at failure is located within the safe area defined by the FAL and the coordinate axes, corresponding to unsafe (non-conservative) assessments. Figure 9 shows graphically the resulting P_{est}/P_{exp} ratios, revealing the safety of the assessments and the reasonable conservatism, with P_{est}/P_{exp} values which are generally between 0.5 and 1.

Interestingly, all the assessment points are located above the $K_r/L_r=1.1$ line, suggesting fracture dominated failures with negligible influence of plastic collapse processes.

The proposed approach, therefore, provides safe estimations of the critical loads for U-notched and V-notched specimens, with a reasonable significant amount of conservatism. The main source of the conservatism may be caused by the low level of constraint of the loaded plates, which are tested under tensile conditions, whereas fracture toughness is obtained from highly constrained specimens (SENB). However, there is a counterintuitive observation: in both U- and V-notches, the conservatism associated to a/W values of 0.50 is higher than that observed in plates with a/W=0.25. Thus, longer defects are providing more conservative assessments, something that contradicts the fact that shorter defects are associated to lower levels of constraint and, theoretically, more conservative FAD assessments. Something similar was observed in [20] for PLA plates, and will require further investigation to determine the real effect of constraint in the geometric and loading conditions analyzed in this work, and the reasons of the higher conservatism observed here for conditions with higher constraint. At this moment the authors have not found a clear explanation.

This being said, it is important to note that the authors have previously shown [19] that the use of fracture toughness results derived from ASTM D6068 [29], and assuming no stable crack propagation before final fracture, may generate non-conservative FAD analyses in additively manufactured polymers, although for this particular material (PLA-Gr) and raster orientation (45/-45), the ASTM D6068 standard provided more accurate results than its linear-elastic equivalent (ASTM 5045 [30]). In case of using [30], the resulting conservatism would be larger. Likewise, the value of K_{mat} used in the analyses (see Table 1) is the average value derived from several fracture tests. In case of using other type of criteria, such as the K_{mat} value associated with a 5% probability of failure, the conservatism would also increase.

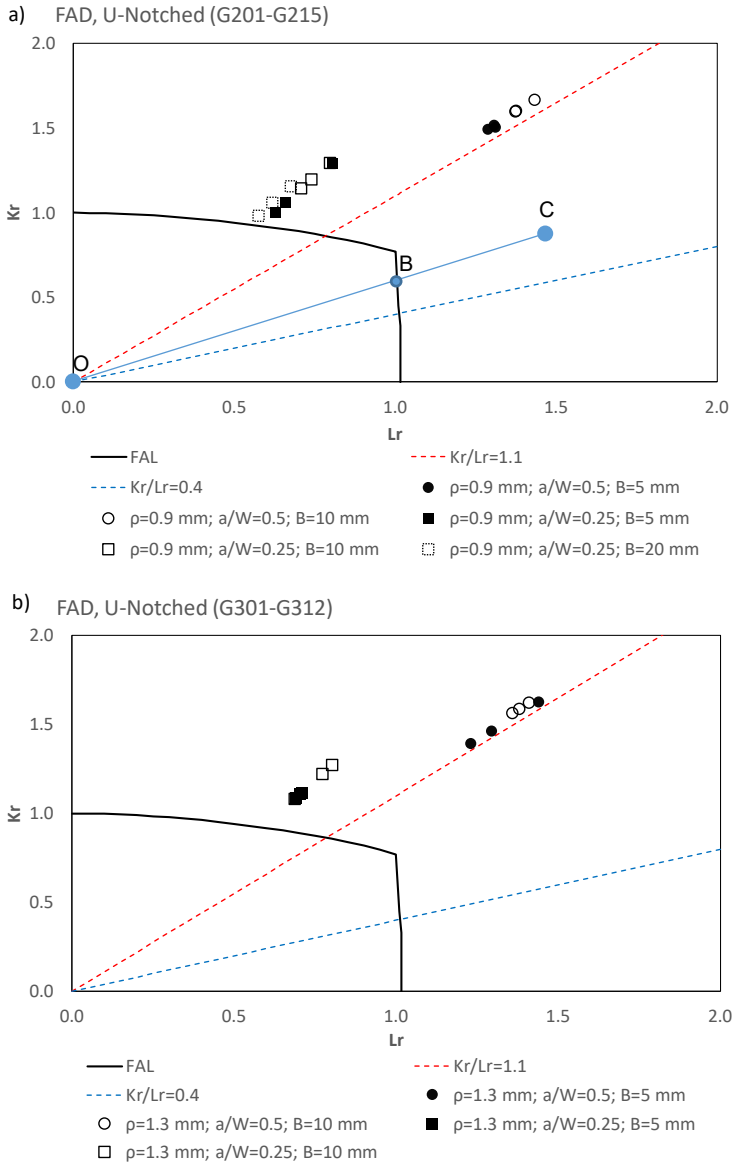

FIGURE 6: FAD ASSESSMENT OF THE U-NOTCHED PLATES. DEFINITION OF THE ESTIMATION OF THE CRITICAL LOADS. GEOMETRICAL PARAMETERS REFER TO NOMINAL VALUES. A) SPECIMENS G201 TO G215; B) SPECIMENS G301 TO G312.

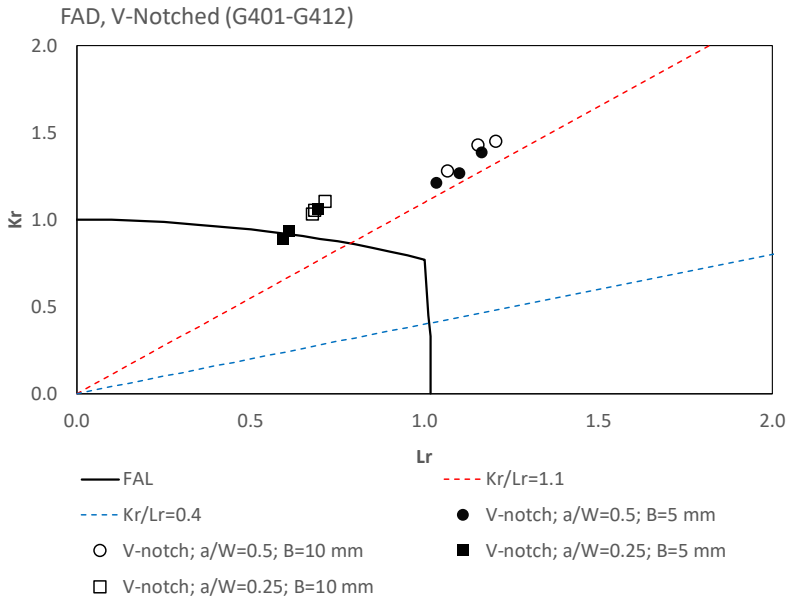

FIGURE 7: FAD ASSESSMENT OF THE V-NOTCHED PLATES. GEOMETRICAL PARAMETERS REFER TO NOMINAL VALUES. SPECIMENS G401 to G412.

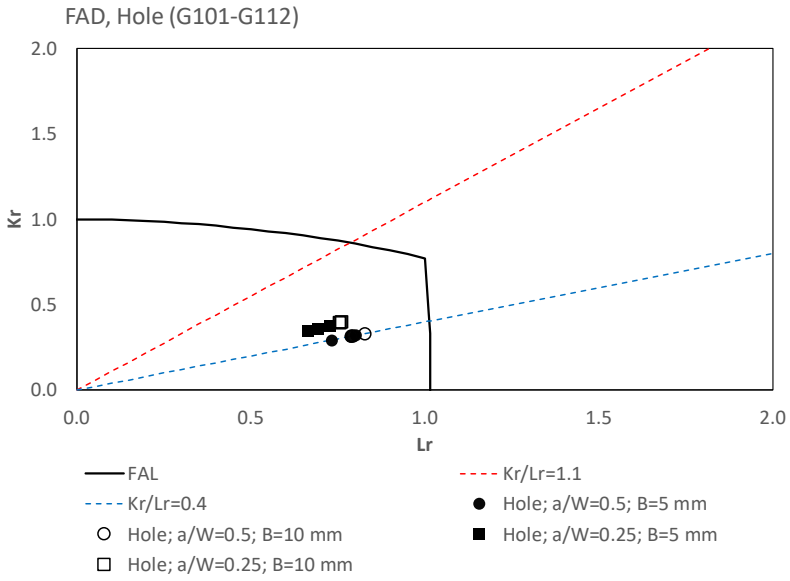

FIGURE 8: FAD ASSESSMENT OF THE PLATES WITH CENTRAL HOLE. GEOMETRICAL PARAMETERS REFER TO NOMINAL VALUES. SPECIMENS G101 TO G112.

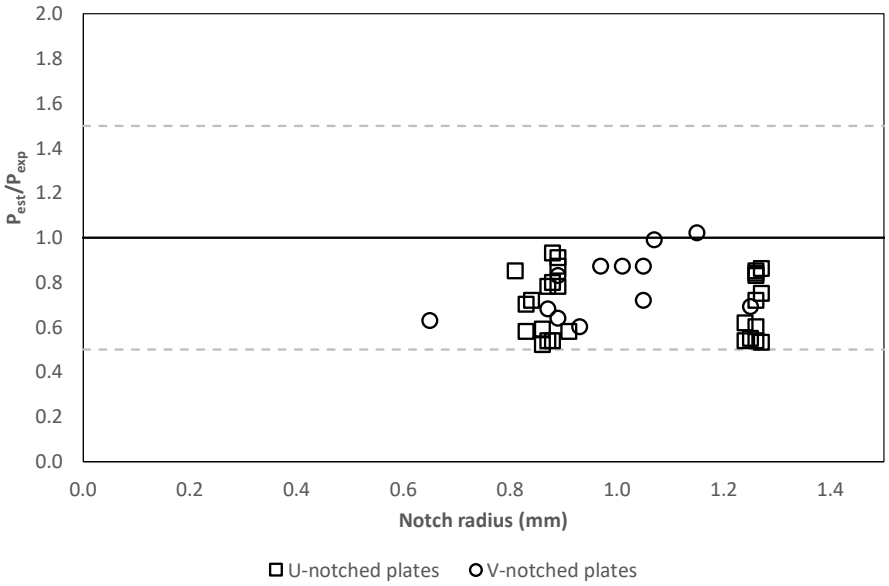

FIGURE 9: P_{EST}/P_{EXP} RATIOS OBTAINED IN U-NOTCHED PLATES AND V-NOTCHED PLATES. NOTCH RADII REFER TO ACTUAL (MEASURED) VALUES.

Concerning the specimens containing central holes, the results are not safe, even with the considerations mentioned above. All the assessment points at failure are located within the safe area, generating P_{est}/P_{exp} values above 1 in all cases. This is in agreement with the results obtained in [20] on PLA material, where the plates containing central holes consumed most (even all) of the conservatism associated to U-notched and V-notched specimens. Further research is needed to completely understand these results, but as commented in [20]:

- The assessment points are located close to the $K_r/L_r = 0.4$ line, signifying plastic collapse dominated failures [28]. Thus, the reasons for the unsafe predictions could be partially related with the plastic collapse analysis itself. In other words, the results obtained in this work suggest that plastic collapse (or limit load) solutions used in traditional materials (e.g., metals, conventionally fabricated polymers, etc.) may be unsafe for additively manufactured materials with numerous internal defects, as is the case of the PLA-Gr material analyzed here. And (or)
- The Creager-Paris stress distribution [25] is valid for slender U-notches. Thus, here, it is being applied outside its validity range when analyzing holes. Consequently, the use of K^N_{mat} estimations derived from the Creager-Paris stress solution may be unsafe for holes.

4. CONCLUSION

This paper evaluates the fracture behavior of fused filament fabrication (FFF) graphene reinforced PLA (PLA-Gr) plates containing different types of notches. The amount of graphene is fixed at 1 wt.%. The assessment methodology is based on the combined application of Failure Assessment Diagrams (FAD) and the notch correction derived from the Line Method (LM), which is one of the different versions of the Theory of Critical Distances (TCD).

The approach has been validated in the material being analyzed through its application to an experimental program composed of 51 plates that combine different types of notches (U-notches, V-notches and circular holes), thicknesses (5 mm to 20 mm), notch length to plate width ratios (a/W), and notch radii (ρ). V-notches and circular holes, which generate less demanding stress fields than U-notches, have been conservatively assumed to behave as U-notches.

The results obtained in this work demonstrate that the proposed approach generates safe conservative estimations of critical loads in U-notched and V-notched plates in this particular composite. This conservatism is, anyhow, similar to that described in the literature, and accepted in practice, for metallic materials subjected to low constraint conditions.

In the case of plates with a central hole, the analysis has provided unsafe predictions of the critical loads. This has been justified by the use of conventional solutions of limit loads, which should be used with caution in this kind of additively manufactured polymeric materials, and/or by the use of the Creager-Paris stress field solution well beyond its validity range.

ACKNOWLEDGEMENTS

This publication is part of the project "Comportamiento en fractura y efecto entalla en compuestos de matriz termoplástica obtenidos por fabricación aditiva, PID2021-122324NBI00" funded by MCIN/AEI/10.13039/501100011033/FEDER "Una manera de hacer

Europa".

REFERENCES

[1] BS 7910:2019, Guide to methods for assessing the acceptability of flaws in metallic structures, British Standard Institution, London, UK, 2019.

[2] API 579-1/ASME FFS-1, Third edition, The American Society of Mechanical Engineers, New York, USA, 2016.

[3] Taylor, D., 2007, *The Theory of Critical Distances*, Elsevier, Oxford, UK.

[4] Cicero, S., Madrazo, V., García, T., Cuervo, J., Ruiz, E., 2013, "On the notch effect in load bearing capacity, apparent fracture toughness and fracture mechanisms of polymer PMMA, aluminium alloy Al7075-T651 and structural steels S275JR and S355J2", *Eng. Fail. Anal.,* 29, 108–121.

[5] Cicero, S., Madrazo, V., García, T., 2014, "Analysis of notch effect in the apparent fracture toughness and the fracture micromechanisms of ferritic-pearlitic steels operating within their lower shelf", *Eng. Fail. Anal.,* 36, 322–342.

[6] Cicero, S., Gutierrez-Solana, F., Horn, A.J., 2009, "Experimental analysis of differences in mechanical behaviour of cracked and notched specimens in a ferritic-pearlitic steel: considerations about the notch effect on structural integrity", *Eng. Fail. Anal.,* 16, 2450–2466.

[7] Sih, G.C., 1974, "Strain-energy-density factor applied to mixed mode crack problems", *Int.J. Fract.,* 10, 305–321.

[8] Cicero, S., Madrazo, Carrascal, I.A., Cicero, R., 2011, "Assessment of notched structural components using failure assessment diagrams and the theory of critical distances", *Eng. Fract. Mech.,* 78, 2809–2825.

[9] Cantrell, J.T., Rohde, S., Damiani, D., Gurnani, R., DiSandro, L., Anton, J., Young, A., Jerez, A. Steinbach, D., Kroese, C. and Ifju, P.J., 2017, "Experimental characterization of the mechanical properties of 3D-printed ABS and polycarbonate parts," *Rapid Prototyp. J.*, 23, pp. 811–824. doi:10.1108/RPJ-03-2016-0042.

[10] Bamiduro, O., Owolabi, G., Haile, M.A. and Riddick, J.C., 2019, "The influence of load direction, microstructure, raster orientation on the quasi-static response of fused deposition modeling ABS," *Rapid Prototyp. J.,* 25, pp. 462–472. doi:10.1108/RPJ-04-2018-0087.

[11] Ahn, S. Montero, M. Odell, D. Roundy, S. and Wright, P.K. 2002, "Anisotropic material properties of fused deposition modeling ABS," *Rapid Prototyp. J.,* 8, pp. 248–257. doi:10.1108/13552540210441166.

[12] Ng, C.T. and Susmel, L., 2020, "Notch static strength of additively manufactured acrylonitrile butadiene styrene (ABS)," *Addit. Manuf.,* 34, 101212. doi:10.1016/j.addma.2020.101212.

[13] Cicero, S., Martínez-Mata, V., Alonso-Estebanez, A., Castanon-Jano, L. and Arroyo, B., 2020, "Analysis of Notch Effect in 3D-Printed ABS Fracture Specimens Containing U-Notches," *Materials*, 13, 4716. doi:10.3390/ma13214716.

[14] Ameri, B., Taheri-Behrooz, F. and Aliha, M.R.M., 2020, "Fracture loads prediction of the modified 3D-printed ABS specimens under mixed-mode I/II loading," *Eng. Fract. Mech*., 235, 107181. doi:10.1016/j.engfracmech.2020.107181.

[15] Mustafa, M.A., Raja S., Asadi, L.A.A.L., Jamadon, N.H., Rajeswari N., Kumar, A.P, 2023, "A Decision-Making Carbon Reinforced Material Selection Model for Composite Polymers in Pipeline Applications," *Adv. Polym. Technol*., 2023, 6344193. doi:10.1155/2023/6344193

[16] Bouzid, A.H. Vafadar, A.K., Ngô, A.D., 2021, "On the Modeling of Anisotropic Fiber-Reinforced Polymer Flange Joints*," J. Pressure Vessel Technol*., 143(6), 061506. doi:10.1115/1.4051365

[17] Fuentes, J.D., Cicero, S., Ibañez-Gutierrez, F.T., Procopio, I., 2018, "On the use of British standard 7910 option 1 failure assessment diagram to non-metallic materials", *Fatigue Fract. Eng. Mater. Struct.,* 41, 146–158.

[18] Martínez, M., Cano, A.J., Salazar, A., Rodríguez, J., 2022, "On the failure assessment diagram methodology in polyamide 12", *Eng. Fract. Mech.,* 269, 108558.

[19] Cicero, S., Sánchez, M., Martínez-Mata, V., Arrieta, S, and Arroyo, B., 2022, "Structural integrity assessment of additively manufactured ABS, PLA and graphene reinforced PLA notched specimens combining Failure Assessment Diagrams and the Theory of Critical Distances," *Theor. Appl. Fract. Mech.,* 121, 103535.

[20] Cicero, S., Arrieta, S., Sanchez, M., Castanon-Jano, L., 2023, "Analysis of additively manufactured notched PLA plates using failure assessment diagrams", *Theor. Appl. Fract. Mech.,* 125, 103926.

[21] Cicero, S., Martínez-Mata, V., Castanon-Jano, L., Alonso-Estebanez, A., Arroyo, B, 2021, "Analysis of notch effect in the fracture behaviour of additively manufactured PLA and graphene reinforced PLA," *Theor. Appl. Fract. Mech.,* 114, 103032.

[22] Valvez, S., Silva, A.P., Reis, N.B., 2022, "Optimization of printing parameters to maximize the mechanical properties of 3D-printed PETG-based parts", *Polymers*, 14, 2564.

[23] Miller, A.G., 1988, Review of limit loads of structures containing defects, Int. J. Press. Vessel Pip. 32, 197–327.

[24] Horn, A.J., Sherry, A.H., 2012, "An engineering assessment methodology for non-sharp defects in steel structures- Part I: procedure development", *Int. J. Press. Vessel. Pip.*89, 137–150.

[25] Creager, M. and Paris, P.C., 1967, "Elastic field equations for blunt cracks with reference to stress corrosion cracking," *Int. J. Fract. Mech.,* 3, pp. 247–252.

[26] Lazzarin, P., Berto, F., 2015, Some expressions for the strain energy in a finite volume surrounding the root of blunt V-notches, *Int. J. Fract.* 135, 161–185.

[27] Anderson, T.L., 2005, *Fracture Mechanics: Fundamentals and Applications*, 4th ed., CRC Press, Boca Raton, FL, USA.

[28] Kocak, M., Webster, S., Janosch, J.J., Ainsworth, R.A., Koers, R., 2008, *FITNET fitness-forservice (FFS) Procedure*, Vol. 1, GKSS Hamburg, Germany.

[29] ASTM D6068-10(2018), Standard Test Method for Determining J-R Curves of Plastic Materials, ASTM International, West Conshohocken, PA, 2018.

[30] ASTM D5045-14, Standard Test Methods for Plane-Strain Fracture Toughness and Strain Energy Release Rate of Plastic Materials, ASTM International, West Conshohocken, PA, 2014.